Journal of Solid State Chemistry 182 (2009) 60–64

Contents lists available at ScienceDirect

Journal of Solid State Chemistry

journal homepage: www.elsevier.com/locate/jssc

# Mössbauer investigation of $^{57}Fe$ doped $La_4Ni_3O_{10\pm y}$ phases

M.D. Carvalho [a,*], A. Wattiaux [b], L.P. Ferreira [c,d], J.M. Bassat [b]

[a] CCMM/Dep. Química e Bioquímica, Faculdade de Ciências, Universidade de Lisboa, Campo Grande, Ed. C8, 1749-016 Lisboa, Portugal
[b] CNRS, Université de Bordeaux, ICMCB, 87 Avenue du Dr. A. Schweitzer, Pessac, F-33608, France
[c] CFMC, Universidade de Lisboa, Campo Grande, Ed. C8, 1749-016 Lisboa, Portugal
[d] Dep. Física, Faculdade de Ciências e Tecnologia, Universidade de Coimbra, 3004-516 Coimbra, Portugal

ARTICLE INFO

*Article history:*
Received 18 July 2008
Received in revised form
29 September 2008
Accepted 4 October 2008
Available online 17 October 2008

*Keywords:*
Ruddlesden–Popper
Mössbauer spectroscopy
Oxygen stoichiometry
Electrical conductivity

ABSTRACT

$^{57}Fe$ doped $La_4Ni_{2.97}Fe_{0.03}O_{9.95}$ was synthesized by a citrate method and, afterwards, successfully oxidized and reduced by electrochemical methods. The compounds obtained were investigated by X-ray diffraction, electrical measurements and Mössbauer spectroscopy. The study allowed to follow the variation of the two nickel sites environment with the oxygen stoichiometry and a deeper understanding of the electrical behavior versus oxygen non-stoichiometry was achieved. The Mössbauer study revealed that after both oxidation and reduction treatments, the major modifications were observed on the octahedra adjacent to the $La_2O_2$ layers, while the middle octahedra of the triple perovskite block remained almost unchanged. The oxygen intercalation (oxidized treatment) takes place essentially in the $La_2O_2$ layers and the oxygen desintercalation (reduction treatment) occurs in the octahedral sites adjacent to those layers.



## 1. Introduction

Over the last two decades, the layered rare earth nickel oxides $Ln_{n+1}Ni_nO_{3n+1}$ (Ln = La, Pr, Nd) have received a renewed attention, specially aiming to achieve a better understanding of their electronic properties. More recently, these compounds, described as Ruddlesden–Popper (RP) type phases, have attracted much attention as alternate cathode materials for solid oxide fuel cells (SOFC), namely those with Ln = La [1–3]. The RP structure of these nickelates is a stacking up of $n$ perovskite-like layers ($LnNiO_3$) separated by rock salt layers (LnO) along the $c$ axis. Thus it can also be written as $(LnO)(LnNiO_3)_n$, and its dimensional character is known to increase with increasing $n$. The first term of this series, $Ln_2NiO_4$ ($n=1$), adopts the 2D-$K_2NiF_4$-type structure while the last term, $LnNiO_3$ ($n=\infty$), exhibits the 3D-perovskite structure.

The $n=3$ compound $Ln_4Ni_3O_{10}$ is composed of three layers of $NiO_6$ octahedra (perovskite block) separated by a rock-salt layer ($Ln_2O_2$), as represented in Fig. 1. In this structure, the nickel ions of the middle octahedra (in a perovskite type surrounding) correspond to a crystallographic site (site I) slightly different from the other two, adjacent to the $Ln_2O_2$ layers (site II). These compounds are depicted as having 1/3 of $Ni^{2+}$ and 2/3 of $Ni^{3+}$ and the metal to metal transition observed at 140 (Ln = La), 145 (Ln = Pr) and 165 K (Ln = Nd) motivated the study of their electronic properties. It was suggested that these anomalies were due to charge ordering phenomenon, charge-density wave driven instabilities or charge-transfer gap [4–6], even if no clear evidence of these phenomena has been presented so far. However, some discrepancies reported on the temperature values of the electrical transitions for the different compounds can be related to the different oxygen content of the samples. Indeed, using electrochemical methods, it was possible to demonstrate that changes on the oxygen content of an as-prepared $La_4Ni_3O_{10.02}$ sample induced consistent variations on the electrical behavior of the resulting compounds [7,8]. Particularly, it was demonstrated that the metal to metal transition observed around 140 K in the as-prepared sample disappears when the sample is oxidized, its electrical behavior becoming similar to that of the perovskite phase $LaNiO_3$. On the contrary, an enhancement of the metal to metal transition is observed when the sample is reduced. Therefore, the oxygen stoichiometry is a critical parameter strongly influencing the electronic properties of the compounds, for which the general formula can be written as $La_4Ni_3O_{10+y}$ (with $y>0$ or $y<0$).

In the present work, a Mössbauer investigation of $^{57}Fe$ doped $La_4Ni_{2.97}Fe_{0.03}O_{10\pm y}$ ($n=3$) has been performed at 293 K. In order to obtain samples with different oxygen contents, the as-prepared compound was submitted to electrochemical treatments, as previously reported for the undoped one $La_4Ni_3O_{10}$ [7]. The purpose was to follow the evolution of the two Ni sites and their dependence on the oxygen stoichiometry, in order to achieve a better understanding of the correlation between transport properties and $Ni^{2+}/Ni^{3+}$ ratio. Results of XRD and electrical resistivity measurements are also reported.

* Corresponding author. Fax: +351 21 750 00 88.
*E-mail address:* mdcarvalho@fc.ul.pt (M.D. Carvalho).

0022-4596/$ - see front matter © 2008 Elsevier Inc. All rights reserved.
doi:10.1016/j.jssc.2008.10.006

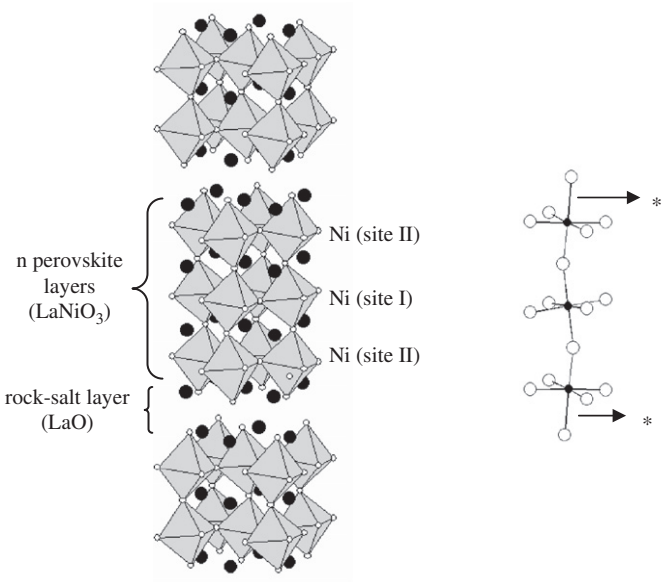


**Fig. 1.** Structure of the $La_4Ni_3O_{10}$ based on previously reported results obtained by neutron diffraction [11], and schematic representation of the bonds between nickel and oxygen in the perovskite block. (*): Larger Ni–O bond lengths. The octahedra represent $NiO_6$, the small open circles and the solid circles represent oxygen and lanthanum, respectively.

## 2. Experimental

The as-cast sample was prepared according to the citrate method previously described for $La_4Ni_3O_{10+y}$ [9]. In order to dope the nickelate with $^{57}Fe$ and obtain $La_4Ni_{2.97}Fe_{0.03}O_{10}$, a stoichiometric mixture of $La_2O_3$ (beforehand dried in air at 1123 K for 15 h), NiO and $^{57}Fe$ (Eurisotop, 95.9%) was dissolved in nitric acid ($HNO_3$:$H_2O$, 1/3:2/3) followed by the addition of citric acid. This solution was slowly dried on a sand bath which induced autocombustion. The product was first annealed at 1173 K for 2 h in air, followed by a thermal treatment in air, at 1353 K for 60 h, with intermittent grindings.

In order to oxidize and reduce the $^{57}Fe$ doped phase, electrochemical treatments were carried out using the galvanostatic method ($I = 20\,\mu A$) for the oxidation process and the potentiostatic method ($E = -0.025\,V$) for the reduction one, as previously reported for the nickelate $La_4Ni_3O_{10.02}$ phase [7]. These reactions were performed on pellets of the as-prepared $^{57}Fe$ doped compound, using a one compartment cell in a 1 mol $dm^{-3}$ KOH solution [7].

The samples were characterized by powder X-ray diffraction (XRD) using a Philips diffractometer with Cu$K\alpha$ radiation calibrated with a Si standard, before and after the electrochemical treatment. The XRD patterns were obtained for $2\theta$ between 20° and 120° in steps of 0.02° and analyzed by Rietveld refinement using the FullProf program [10]. However, since the electrochemically treated compounds did not allow a precise structure determination due to the adsorption of some electrolyte, the refinements were only carried out in order to determine more precisely the cell parameters values of the different samples. A polynomial function was used to model the background level. Peak shapes were fitted using a pseudo-Voigt function. In these refinements, the positions of all species were fixed, considering the structural determination previously reported and obtained by neutron powder diffraction [11].

The oxygen content of the as-prepared compounds was calculated after iodometric titration of the $M^{3+}$ ions ($Fe^{3+}$ and $Ni^{3+}$). Similar chemical analysis of the samples after the electrochemical treatment did not allow reliable results due to some electrolyte adsorption.

Electrical resistivity measurements were performed in the temperature range between 5 and 300 K using a conventional four-probe method.

Mössbauer spectra were collected at room temperature using a Halder type transmission Mössbauer spectrometer with conventional constant acceleration and a $^{57}Co$ source in a Rh matrix. The analysis of the spectra was carried out in two steps. Initially, the spectra were fitted to Lorentzian lines, allowing to refine the position, amplitude and width of each line. The experimental hyperfine parameters of the different iron sites were deduced from this first approach. In a second stage, the calculation was performed by stripping the spectra in terms of distribution of the hyperfine parameters by the method of Hesse and Rubartsch [12]. This method is often used for disordered compounds characterized by a broad distribution of possible environments, leading to experimental spectra with lines of significant width and profiles deviated from a Lorentzian line. Isomer shifts are expressed with respect to $\alpha$-iron at 293 K.

## 3. Results and discussion

### 3.1. Structural and electrical characterization of the compounds

#### 3.1.1. As-prepared compounds

XRD results indicate that pure phases with the Ruddlesden–Popper structure were obtained for both $La_4Ni_3O_{10+y}$ and $^{57}Fe$ doped samples. Table 1 presents the cell parameters values obtained after the XRD refinement of the as-prepared compounds, as well as the amounts of $y$ calculated using the iodometric titration data. From these results, it can be deduced that the substitution of nickel by iron induces the reduction of some $Ni^{3+}$ ions, resulting in oxygen deficiency for the doped compound ($y = -0.05$), while a slight oxygen excess ($y = +0.05$) was determined for the non-doped sample. The reduction of $Ni^{3+}$ ions induced by the nickel substitution by iron was already reported for $LaNi_{1-x}Fe_xO_3$ compounds [13].

The dependence of the electrical resistivity on the temperature for both compounds is presented in Fig. 2. Although the transition around 140 K is observed for both compounds, it is more accentuated for the $^{57}Fe$ doped sample, in good agreement with the lower oxygen content of this sample (calculated by titration data) and our previous studies [8].

#### 3.1.2. Oxidized and reduced compounds

After the electrochemical treatment, the resistivity measurements were performed on the washed pellets. For the XRD and Mössbauer measurements, powder samples of the pellets were used. Fig. 3 presents the XRD patterns of the reduced and oxidized compounds, as well as the one of the as-prepared $^{57}Fe$-doped sample for better comparison. The XRD analysis reveals that the Ruddlesden–Popper structure was maintained with a small variation on the cell parameters (Table 2). As can be seen, the oxidation treatment led to a decrease of the cell volume, while a small increase was observed in the case of the reduced compound,

**Table 1**
Cell parameters values obtained by Rietveld refinement of the XRD patterns and results of the iodometric titration of the as-prepared compounds

| | $y$ | $a$/Å | $b$/Å | $c$/Å | Vol/Å$^3$ |
|---|---|---|---|---|---|
| $La_4Ni_3O_{10+y}$ | +0.05 | 5.4109(3) | 5.4616(3) | 27.967(2) | 826.5(1) |
| $La_4Ni_{2.97}Fe_{0.03}O_{10+y}$ | −0.05 | 5.4118(3) | 5.4630(3) | 27.964(2) | 826.7(1) |

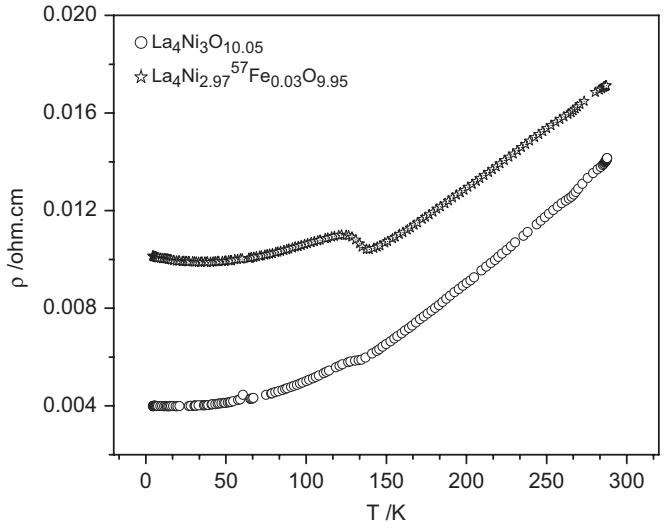


**Fig. 2.** Thermal electrical resistivity dependence of the as-prepared compounds.

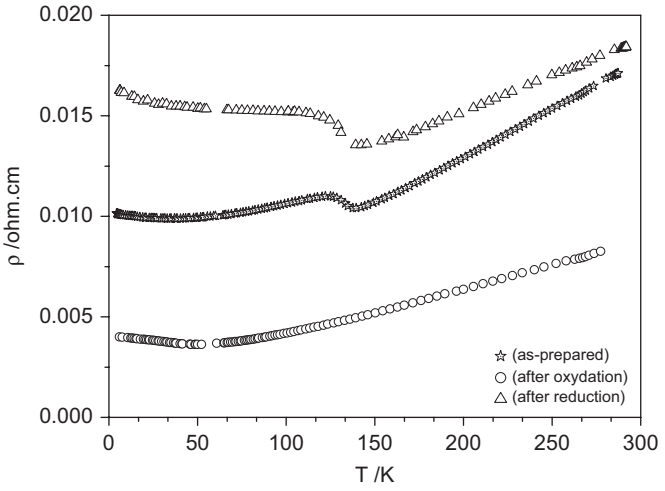


**Fig. 4.** Thermal electrical resistivity dependence for the $^{57}$Fe (3%) doped compounds before and after electrochemical treatment.

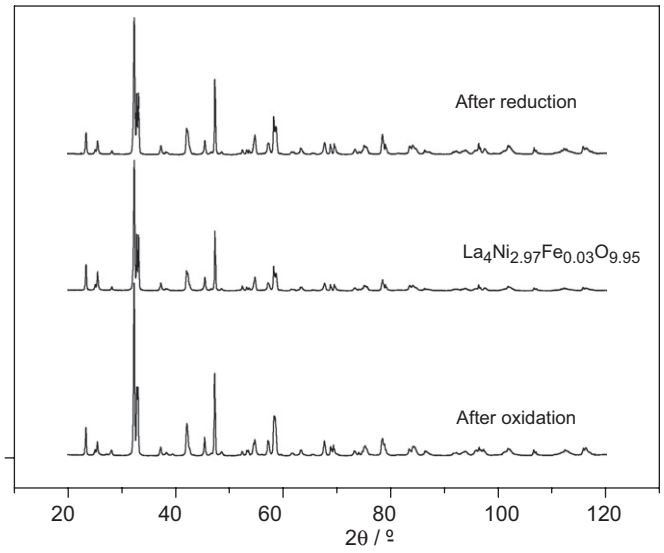


**Fig. 3.** XRD patterns of the doped compounds (as-prepared $La_4Ni_{2.97}Fe_{0.03}O_{9.95}$, oxidized and reduced).

**Table 2**
Cell parameters values obtained by Rietveld refinement of the XRD patterns for the as-prepared, oxidized and reduced samples

| | $a$/Å | $b$/Å | $c$/Å | Vol/Å$^3$ |
|---|---|---|---|---|
| $La_4Ni_{2.97}Fe_{0.03}O_{9.95}$ | 5.4118(3) | 5.4630(3) | 27.964(2) | 826.7(1) |
| After oxidation ($I = 20\,\mu A$) | 5.4133(4) | 5.4478(4) | 27.916(2) | 823.3(1) |
| After reduction ($E = -0.025\,V$) | 5.4144(2) | 5.4649(2) | 27.971(1) | 827.6(1) |

in accordance with results already published for undoped compounds [7]. These variations are well understood considering the increase of (i) the $Ni^{3+}$ content for the oxidized compound and (ii) the $Ni^{2+}$ content for the reduced one, as the $Ni^{2+}$ radius (0.69 Å) is higher than the $Ni^{3+}$ one (0.56 Å). It can also be inferred that the oxidation led to a less orthorhombic strain, as $b$ and $a$ cell parameters become closer in the oxidized compound.

Fig. 4 presents the thermal resistivity behavior of all $^{57}$Fe doped samples. As for $La_4Ni_3O_{10\pm y}$ compounds [8], the results clearly indicate a straight relation between the transition observed around 140 K and the oxygen stoichiometry of the sample. For the oxidized sample, the anomaly disappears and the compound displays metallic type behavior, whereas the electrical resistivity of the reduced compound is enhanced and shows a more pronounced metal to metal transition.

### 3.2. $^{57}$Fe Mössbauer spectroscopy of the $La_4Ni_{2.97}{}^{57}Fe_{0.03}O_{10\pm y}$ compounds

#### 3.2.1. As-prepared compound

The Mössbauer spectrum of the as-prepared compound is shown in Fig. 5 and the results of the fitting procedure are presented in Table 3. As can be seen, the spectrum is well resolved using two distributions of quadrupole splittings with line width values fixed at $\Gamma = 0.20\,mm\,s^{-1}$, indicating that the iron ions occupy two distinct crystallographic sites, as expected since two different octahedral sites exist in the $n = 3$ RP structure (Fig. 1). The calculation using distributions of the hyperfine parameters is justified by the chemical disorder around the iron ions due to the presence of $Ni^{2+}$ and $Ni^{3+}$ and, therefore, to different Fe–O bond lengths in the environments of the two $^{57}$Fe sites. Even if not detected by XRD, the presence of some traces of $Fe_2O_3$ cannot be disregarded in the Mössbauer spectra. However, it was considered that such minor quantity (less than 1% of the total 3% of $^{57}$Fe) do not affect the electrical results or the conclusions of this work.

The isomer shift values ($\delta$) obtained (Table 3) cannot be attributed to the presence of $Fe^{2+}$ ($\delta > 1\,mm\,s^{-1}$) or $Fe^{4+}$ ($\delta \approx 0.00\,mm\,s^{-1}$) although they are smaller than the expected values for octahedral $Fe^{3+}$ ions ($\delta \approx 0.36\,mm\,s^{-1}$) [14]. The $\delta$ values obtained in the present study are similar to those reported by Khim et al. (between 0.22 and 0.26 $mm\,s^{-1}$) for the $^{57}$Fe doped perovskites $LnNi_{0.98}Fe_{0.02}O_3$ (Ln = Pr, Nd and Sm) [15]. It is generally known that $Ni^{3+}$–O bonds are more covalent than $Fe^{3+}$–O ones. Therefore, in such microdoped nickelates where iron ions are surrounded by $Ni^{3+}$ ions, Khim et al. suggested that the metal site environment has a pronounced covalent character, leading to a decrease of the isomer shift values for $^{57}Fe^{3+}$ ions. Such explanation can also be considered in the present work, where similar compounds are investigated justifying, therefore, the attribution of the obtained values of isomer shifts (0.26 and 0.30 $mm\,s^{-1}$) to the presence of $Fe^{3+}$ ions in octahedral sites.

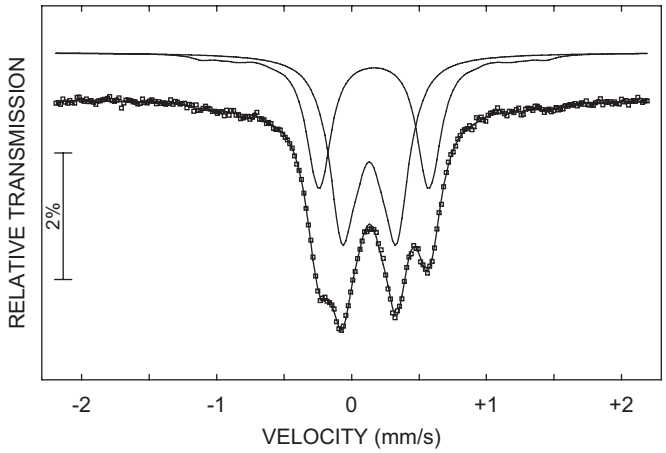


**Fig. 5.** Mössbauer spectra of the as-prepared $La_4Ni_{2.97}Fe_{0.03}O_{9.95}$ compound.

**Table 3**
Results of the calculated Mössbauer spectra for the different compounds

| | Site | $\delta$/mm s$^{-1}$ | $\Gamma$/mm s$^{-1}$ | $\Delta$/mm s$^{-1}$ | % ($\pm$2) |
|---|---|---|---|---|---|
| As-prepared | DIS1 | 0.26(1) | 0.20 | 0.43(2) | 58 |
| $^{57}$Fe (3%) | DIS2 | 0.30(1) | 0.20 | 0.95(2) | 42 |
| Oxidized | DIS1 | 0.26(1) | 0.20 | 0.40(2) | 62 |
| | DIS2 | 0.30(1) | 0.20 | 0.87(2) | 38 |
| Reduced | DIS1 | 0.22(1) | 0.25 | 0.39(2) | 60 |
| | DIS2 | 0.28(1) | 0.25 | 0.58(2) | 40 |

$\delta$: isomer shift; $\Delta$: quadrupole splitting; $\Gamma$: line width.

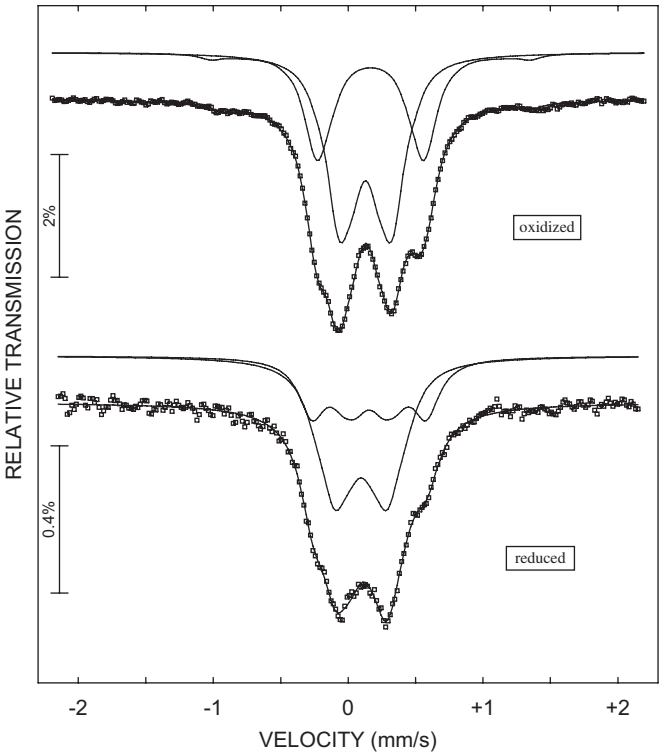


**Fig. 6.** Mössbauer spectra of the oxidized and reduced compounds.

In previously reported neutron diffraction studies [11,16], the structure determination of $La_4Ni_3O_{10}$ compounds indicated a Ni–O mean bond length for the middle octahedra (site I in Fig. 1) smaller than the one obtained for the octahedra near the $La_2O_2$ layer (site II in Fig. 1). These works also clearly showed that the octahedra of site I are more regular than those of site II, for which six different Ni–O bond lengths were obtained, one of them being significantly larger (~2.2 Å) than the others. It has also to be taken into account that a smaller Ni–O bond length can be correlated to a higher covalent bond character, corresponding to a smaller isomer shift value. Moreover, the less symmetric octahedra should be associated to a higher quadrupole splitting value ($\Delta$). Therefore, the $^{57}$Fe sites DIS1 and DIS2 presented in Table 3 can be indexed to $Fe^{3+}$ ions in site I and to $Fe^{3+}$ ions in site II (Fig. 1), respectively.

Finally, the population obtained for both sites indicate a clear preference of $Fe^{3+}$ for site I which only corresponds to 1/3 of the total available sites. This result is in good agreement with the easy synthesis of $La_2MO_{4+y}$ compounds when $M = Ni$, which is not the case for $M = Fe$; from this, it can be concluded that nickel ions accommodate better than iron in site II, justifying the higher occupation of site I by iron. Such occupancy preference by iron was also suggested in a previous published work on $Sr_4Mn_{3-x}Fe_xO_{10-y}$ samples [17].

### 3.2.2. Oxidized and reduced compounds

The Mössbauer spectra and the results obtained from the fitting procedure for both oxidized and reduced samples are presented in Fig. 6 and Table 3, where it can be seen that the occupation (%) of both sites is maintained.

Concerning the oxidized sample, the results clearly indicate that the iron sites environment did not suffer significant changes, implying that the electrochemical treatment induced mainly the oxidation of $Ni^{2+}$ rather than $Fe^{3+}$. The slight decrease observed in the quadrupole splitting values of the oxidized compound (specially for DIS2) indicates a more symmetric environment of the octahedral iron sites, in agreement with the orthorhombic strain release observed for this sample. It is well known that interstitial oxygen of the $La_2NiO_{4+y}$ compound is localized in the $La_2O_2$ layers and that a decrease of the Ni–O bond length is observed along the $c$-axis when $y$ increases [18,19]. Such variation of the apical Ni–O bond of nickel ions localized in site II of the RP compound may account for DIS2 quadrupole splitting variation in the oxidized compound, since this one is precisely the bond length significantly larger than the other ones, as previously mentioned.

The oxygen insertion in the $La_2O_2$ layers of the $La_2NiO_{4+y}$ compound determine the decrease observed on the electrical conductivity of this $n = 1$ RP compound when $y$ increases [18,19]. On the contrary, the oxidation of $La_4Ni_{2.97}Fe_{0.03}O_{9.95}$ clearly plays a different role on the electrical behavior of the corresponding compound, which behaves similarly to the perovskite $LaNiO_3$ and not to $La_2NiO_{4+y}$. These observations allow to suggest that, although in a small amount, the oxygen vacancies present on the as-prepared $La_4Ni_{2.97}Fe_{0.03}O_{9.95}$ may be occupied after the oxidation treatment, also contributing to the observed change of the electrical behavior. This hypothesis would increase the 3D-dimensionality of the perovskite block, giving rise to the disappearance of the electrical anomaly around 140 K, as effectively observed.

In the case of the reduced sample, the Mössbauer spectrum reveals some changes in the hyperfine parameters for both sites. It is important to note that the spectrum calculation for this sample was only possible using a line width value ($\Gamma = 0.25$ mm s$^{-1}$) larger than the previous one used for the other samples (0.20 mm s$^{-1}$). This is well explained by an increase of the chemical disorder around the iron ions due to the reduction of some $Ni^{3+}$ ions to $Ni^{2+}$, and the consequent creation of additional oxygen vacancies.

The isomer shift values ($\delta$) obtained for both sites indicate once again that no $Fe^{2+}$ ions were formed, since a decrease on the oxidation number of iron should led to an increase of this parameter. The slight decrease observed on the $\delta$ values of both sites allows to conclude that $Fe^{3+}$ ions coordination definitely did not change. The variation on the $\delta$ values can then be better explained by the increase of $Ni^{2+}$ ions amount (relatively to $Ni^{3+}$) in the $Fe^{3+}$ ions environment. As previously referred, the presence of the $Ni^{3+}$–O bonds, more covalent than the $Fe^{3+}$–O ones induce a diminishing of the isomer shift values for $^{57}Fe^{3+}$ ions in microdoped samples. As $Ni^{2+}$–O bonds are still more covalent than $Ni^{3+}$–O bonds it is not surprising to observe a decrease on the isomer shift of the reduced sample.

The drastic decrease observed on the quadrupole splitting of site DIS2 (site II in Fig. 1), can be interpreted as a consequence of the $Ni^{3+}$ to $Ni^{2+}$ reduction around the iron ions in this site. Due to the similarity between the $Ni^{2+}$ (0.69 Å) and $Fe^{3+}$ (0.65 Å) ionic radii, the $Ni^{3+}$ reduction leads to more symmetric environments around $^{57}Fe$, inducing the decrease of the quadrupole splitting parameter. As a consequence of this preferential reduction, oxygen vacancies would be essentially localized on the (a, b) plane of $Ni^{2+}$ ions of site II. In the case of site DIS1, the practically unchanged value can only be understood if $^{57}Fe$ in site I maintains essentially its environment, suffering only the influence of the $Ni^{2+}$ ions located along the c-axis direction, and assuming that the nickel ions reduction occurs preferentially in the octahedra adjacent to the $La_2O_2$ layers (site II), where oxygen vacancies should be localized.

## 4. Conclusions

In this work, a $^{57}Fe$ doped $La_4Ni_{2.97}Fe_{0.03}O_{9.95}$ compound was successfully oxidized or reduced, the corresponding structural and chemical variations obtained being investigated by powder X-ray diffraction, electrical measurements and Mössbauer spectroscopy.

The results obtained for the two as-prepared compounds ($La_4Ni_3O_{10.05}$ and $La_4Ni_{2.97}Fe_{0.03}O_{9.95}$) showed that the iron doping induces a small decrease of the oxygen content and an increase of the electrical resistivity, highlighting the transition observed around 140 K. Although the $^{57}Fe$ probe seems to preferentially occupy site I, it effectively substitutes the nickel ions in both sites, allowing to follow the nickel environment changes after oxidation or reduction and its correlation with the electronic transition at 140 K.

Only $^{57}Fe^{3+}$ ions were detected in all studied samples, indicating that the reduction and oxidation processes essentially affects the $Ni^{2+}/Ni^{3+}$ ratio. The comparison between Mössbauer results of the as-prepared and oxidized samples suggests that oxygen insertion takes place essentially in the $La_2O_2$ layers, having a minor influence on the Mössbauer probe. In the reduced sample, no evidence of a change on the iron octahedral sites coordination was found, although a significant variation of the quadrupole splitting characterizing site II was observed. These results led us to the conclusion that the oxygen vacancies of the reduced compound are mainly present in the nickel environment localized in site II, influencing indirectly the iron hyperfine parameters.

Although agreeing that the present study is not as conclusive as expected, the authors would like to suggest the existence of a double non-stoichiometry in the $n = 3$ Ruddlesden–Popper compound. We propose that some oxygen vacancies ($x$) are localized essentially around nickel in site II, co-existing with an excess of oxygen ($z$) localized on the $La_2O_2$ layer, the general formula $La_4Ni_3O_{10-x+z}$ being in this case more appropriate. Here, $x$ refers to the sub-stoichiometry related to oxygen vacancies of the same type as found in $LaNiO_{3-x}$. Thus, when $x$ decreases the electrical conductivity increases. The over-stoichiometry $z$ is of the same type as found in $La_2NiO_{4+z}$ and, in this case, when $z$ increases the electrical conductivity decreases. The existence of this double non-stoichiometry may justify the complex electrical behavior found on the $n = 3$ RP compounds, the oxygen content dependence and the different interpretations suggested in the literature for the origin of the electrical anomaly observed around 140 K.

In order to check this hypothesis, we suggest additional experiments such as neutron diffraction on oxidized and reduced samples.

## Acknowledgment

This work was partially supported by the exchange scientific program GRICES (Portugal)/CNRS (France), 2005–2006.

## References

[1] G. Amow, I.J. Davidson, S.J. Skinner, Solid State Ionics 177 (2006) 1205–1210.
[2] G. Amow, S.J. Skinner, J. Solid State Electrochem. 10 (2006) 538–546.
[3] X. Weng, P. Boldrin, I. Abrahams, S.J. Skinner, S. Kellici, J.A. Darr, J. Solid State Chem. 181 (2008) 1123–1132.
[4] Y. Kobayashi, S. Tsniguchi, M. Kasai, M. Sato, T. Nishioka, M. Kontani, J. Phys. Soc. Jpn. 65 (1996) 3978–3982.
[5] G. Wu, J.J. Neumier, M.F. Hundley, Phys. Rev. B 63 (2001) 245120–245125.
[6] Z. Zhang, M. Greenblatt, J. Solid State Chem. 117 (1995) 236–246.
[7] M.D. Carvalho, A. Wattiaux, J.M. Bassat, J.C. Grenier, M. Pouchard, M.I. da Silva Pereira, F.M.A. Costa, J. Solid State Electrochem. 7 (2003) 700–705.
[8] M.D. Carvalho, M.M. Cruz, A. Wattiaux, J.M. Bassat, F.M.A. Costa, M. Godinho, J. Appl. Phys. 88 (2000) 544–549.
[9] M.D. Carvalho, F.M.A. Costa, I.S. Pereira, A. Wattiaux, J.M. Bassat, J.C. Grenier, M. Pouchard, J. Mater. Chem. 7 (1997) 2107–2111.
[10] T. Roisnel, J. Rodriguez-Carvajal, FullProf Suite, April 2005.
[11] C.D. Ling, D.N. Argyriou, G. Wu, J.J. Neumeier, J. Solid State Chem. 152 (1999) 517–525.
[12] J. Hesse, A. Rubartsch, J. Phys. E 7 (1974) 526.
[13] A.E. Goeta, G.F. Goya, R.C. Mercader, G. Punte, H. Falcón, R. Carbonio, Hyperfine Interact. 90 (1994) 371–375.
[14] N.N. Greenwood, T.C. Gibb, Mössbauer Spectroscopy, Chapman and Hall, London, 1971, p. 91.
[15] S.-J. Kim, I. Presniakov, G. Demazeau, K. Poklolok, A. Baranov, A. Sobolev, D. Pankratov, N. Ovanesyan, J. Solid State Chem. 168 (2002) 126–133.
[16] V.I. Voronin, I.F. Berger, V.A. Cherepanov, L.Y. Gavrilova, A.N. Petrov, A.I. Ancharov, B.P. Tolochko, S.G. Nikitenko, Nucl. Instrum. Methods Phys. Res. A 470 (2001) 202–209.
[17] I. Fawcett, G.M. Veith, M. Greenblatt, M. Croft, I. Nowik, J. Solid State Chem. 155 (2000) 96–104.
[18] A. Demourgues, A. Wattiaux, J.C. Grenier, M. Pouchard, J.L. Soubeyroux, J.M. Dance, P. Hagenmuller, J. Solid State Chem. 105 (1993) 458–468.
[19] J.D. Jorgensen, B. Dabrowski, S. Pei, P.R. Richards, D.G. Hinks, Phys. Rev. B 40 (1989) 2187–2199.